CHEMISTRY
A EUROPEAN JOURNAL

DOI: 10.1002/chem.200701344

Reaction Mechanism of Apocarotenoid Oxygenase (ACO): A DFT Study

Tomasz Borowski,*[a] Margareta R. A. Blomberg,[b] and Per E. M. Siegbahn[b]

Abstract: The mechanism of the oxidative cleavage catalyzed by apocarotenoid oxygenase (ACO) was studied by using a quantum chemical (DFT: B3LYP) method. Based on the available crystal structure, relatively large models of the unusual active-site region, in which a ferrous ion is coordinated by four histidines and no negatively charged ligand, were selected and used in the computational investigation of the reaction mechanism. The results suggest that binding of dioxygen to the ferrous ion in the active site promotes one-electron oxidation of carotenoid leading to a substrate radical cation and a Fe-bound superoxide radical. Recombination of the two radicals, which can be realized in at least two different ways, yields a reactive peroxo species that subsequently evolves into either a dioxetane or an epoxide intermediate. The former easily decays into the final aldehyde products, whereas the oxidation of the epoxide to the proper products of the reaction requires involvement of a water molecule. The calculated activation barriers favor the dioxetane mechanism, yet the mechanism involving the epoxide intermediate cannot be ruled out.

Keywords: carotenoids · density functional calculations · oxygenase · reaction mechanisms

Introduction

Carotenoids are natural fat-soluble pigments found in numerous fruits and vegetables, and play multiple protective and regulatory roles in plant and animal physiology.[1,2] For example, β-carotene is used by animals as a precursor of vitamin A, which is indispensable for growth, embryonal development, and visual function. Retinal (vitamin A), like some other biologically important compounds, belongs to a group of apocarotenoids that are synthesized from the parent carotenoids by the oxidative cleavage reaction catalyzed by a family of iron-dependent enzymes.[1,3] Existence of specific carotenoid oxygenases was postulated as early as 1965,[4] however, the identification of the first member of this group, named VP14, was accomplished first in 1997.[5] VP14 is a plant enzyme responsible for the oxidative cleavage of 9-*cis*-violaxanthin (Scheme 1A), the first step in the biosynthesis of abscisic acid, a plant-growth regulator.

In animals, two kinds of β-carotene oxygenases have been identified. First, β-carotene 15,15′-dioxygenase (β-CD) that catalyzes the symmetric cleavage of β-carotene into two molecules of retinal (Scheme 1B), was identified in *Drosophila melanogaster*, mouse, and chicken.[6–9] Second, an enzyme responsible for an asymmetric cleavage of β-carotene to β-*apo*-10′-carotenal and β-ionone (β-carotene 9′,10′-dioxygenase, Scheme 1C) was found in mouse.[10] Carotenoid oxygenase was also identified in cyanobacterium *Synechocystis* sp. PCC 6803, however, this retinal synthesizing enzyme (apocarotenoid oxygenase, ACO) converts β-*apo*-carotenals(ols) and not β-carotene (Scheme 1D).[11] Further information concerning biological and commercial roles of carotenoid cleavage enzymes and products can be found in recent reviews.[1,3,12–14]

With respect to the mechanism of the reaction catalyzed by carotenoid oxygenases, monooxygenase and dioxygenase mechanisms were proposed based on interpretations of oxygen-labeling experiments. In the study utilizing β-CD from chicken intestinal mucosa, the products of the enzy-

[a] Dr. T. Borowski
Institute of Catalysis and Surface Chemistry
Polish Academy of Sciences
ul. Niezapominajek 8, 30-239 Cracow (Poland)
Fax: (+48) 12-425-1923
E-mail: ncborows@cyf-kr.edu.pl

[b] Prof. M. R. A. Blomberg, Prof. P. E. M. Siegbahn
Department of Physics
Stockholm Center for Physics, Astronomy and Biotechnology
Stockholm University, 10691 Stockholm (Sweden)

Supporting information for this article is available on the WWW under http://www.chemeurj.org/ or from the author: Cartesian coordinates and calculated energies for all ground and transition structures: Figure S1 shows structures of intermediates (**3**, **7**, **8**, **9**) and transition states (**TS2**–**TS7**) for the dioxetane mechanism and **model 1**; Figure S2 shows transition states (**TS8**, **TS10**, **TS11**) for the epoxide mechanism and **model 1**; Figure S3 shows species **II**, **III**, and **IV**; Figure S4 presents intermediates **16** and **17**; Figure S5 depicts **TS16**, **20**, and **TS17**.

WILEY InterScience DISCOVER SOMETHING GREAT
© 2008 Wiley-VCH Verlag GmbH & Co. KGaA, Weinheim

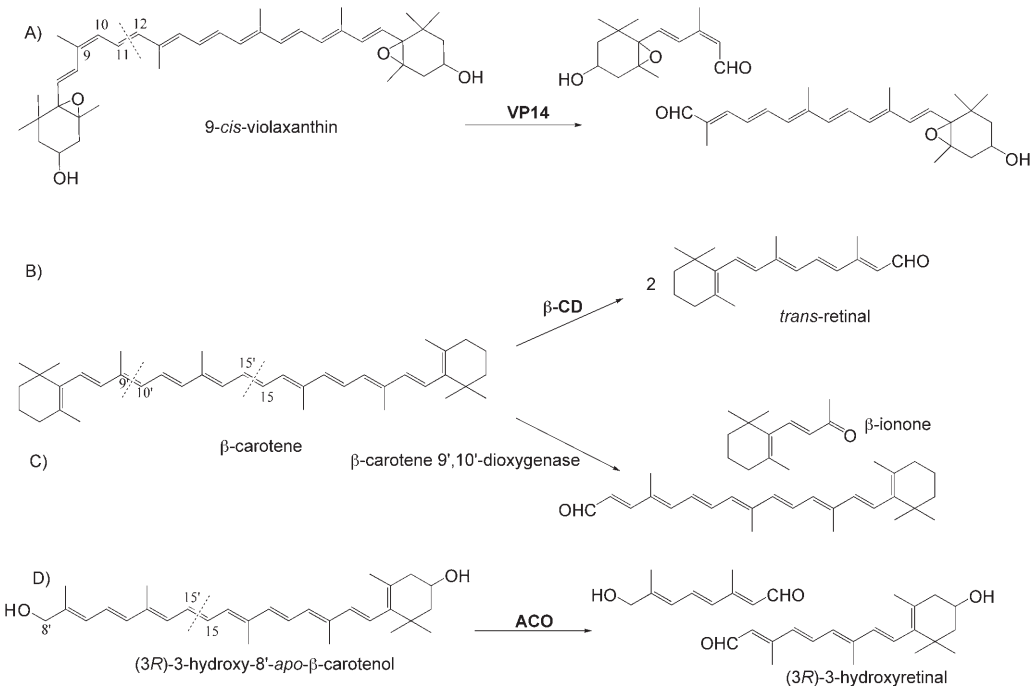

Scheme 1. Reactions catalyzed by selected carotenoid oxygenases.

matic reaction contained almost equal quantities of oxygen derived from O_2 and H_2O, and this result was interpreted as evidence for a monooxygenase mechanism.[15] In the first step of the proposed mechanism, an epoxide is formed with an involvement of the O_2-derived oxygen (Scheme 2).

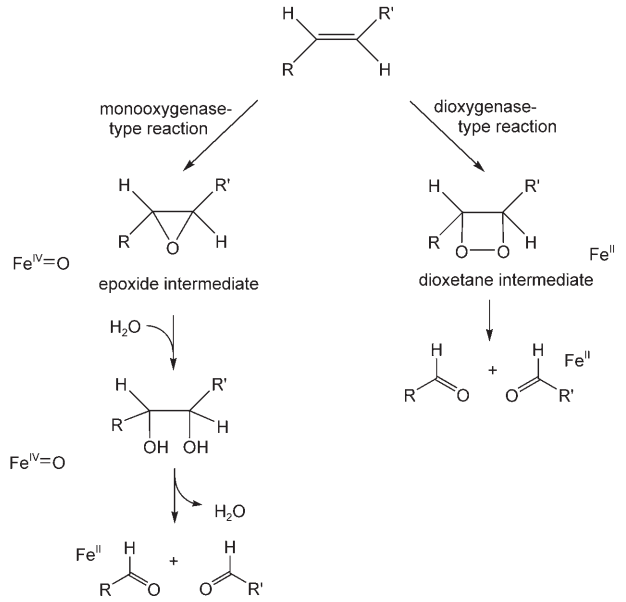

Scheme 2. Two reaction mechanisms proposed for carotenoid oxygenases.

Then, in an unselective ring opening, the epoxide reacts with water yielding a diol intermediate, which is finally oxidatively cleaved to the aldehyde products. The second study used a plant oxygenase (AtCCD1 from *Arabidopsis thaliana*) catalyzing an excentric cleavage of apocarotenoids.[16] In this case, 96% of the ketone (β-ionone) and 27% of the aldehyde product was labeled with O_2-derived oxygen. Moreover, it was shown that under the experimental conditions, aldehyde oxygen readily exchanges with water, and thus, it was claimed that the lower level of the label detected for the aldehyde product is due to such an exchange reaction. These results were proposed to support a dioxygenase reaction mechanism (Scheme 2), in which O_2 adds to the double bond forming a dioxetane intermediate, which subsequently decays to the products. Notably, both of these isotope-labeling experiments have been claimed to be not 100% conclusive.[12]

ACO is the only enzyme from the family of carotenoid oxygenases for which the structural data is currently available.[17] The crystal structure of the ACO–Fe^{II}-substrate ((3*R*)-3-hydroxy-8′-*apo*-β-carotenol) complex, at 2.4 Å resolution, reveals that the ferrous ion is bound by four histidines and one water molecule (Figure 1).

Notably, such a coordination, in which protein provides only histidines to coordinate the ferrous ion, is very rare. Three of these histidines hydrogen-bond with second-shell glutamates. The sixth coordination site (*trans* to His304) remains unoccupied, and it was suggested that this accommodates one oxygen atom of the O_2 molecule when it binds to the active site. Moreover, it was argued that this site is not suitable for a water molecule, because it is lined by the hydrophobic methyl group of Thr136. Most of the substrate molecule, its central part, is visible in the X-ray structure, and it is bound in the extended hydrophobic tunnel passing the Fe^{II} ion. Interestingly, the all-*trans* substrate changes its

 © 2008 Wiley-VCH Verlag GmbH & Co. KGaA, Weinheim

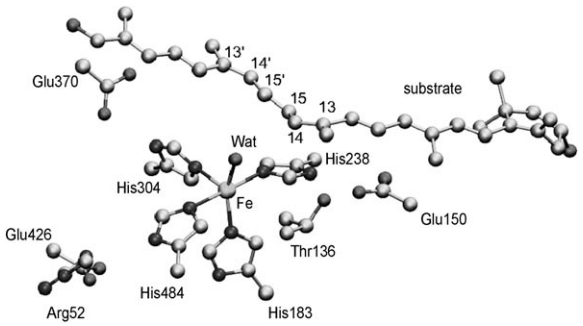

Figure 1. Close-up view of the active-site region in the ACO crystal structure (2BIW).

configuration to *cis* at the two double bonds (C13=C14 and C13′=C14′) flanking the central bond (C15′=C15), which is cleaved by ACO. Based on this structure, it was proposed that dioxygen displaces the water ligand and binds to the ferrous ion side-on occupying the positions *trans* to His183 and His304. The distance between the water ligand and the C15 or C15′ atom of the substrate is around 3.2 Å, and thus, the oxygen atom replacing this water would be in a suitable place for an attack on the substrate.

This report describes a computational study undertaken with the hope to provide new insights into the reaction mechanism of the oxidative cleavage of carotenoids. The computational model was based on the available crystal structure of ACO, and the results suggest that mechanisms involving an epoxide or a dioxetane intermediate have comparable rate-limiting barriers. Thus, it is quite plausible that subtle differences in the architecture of the active sites could fine-tune the reaction energetics, so that one or the other mechanism is favored by a given carotenoid oxygenase. For example, in ACO the presence of the hydrophobic side chain of Thr136 probably favors the side-on binding of dioxygen and the dioxetane mechanism.

Computational Details

Quantum chemical models of the active-site region in the ACO–Fe^{II}-substrate complex were based on the available crystal structure (PDB code: 2BIW). Two models were used, one with a water molecule coordinated to iron (**model 1**), and the second, without this ligand (**model 2**). In all other respects the two models are equivalent. The four histidines coordinated to iron (His183, His238, His304, and His484) were modeled with methylimidazoles, whereas the second-shell glutamates (Glu150 and Glu370), that hydrogen-bond to His238 and His304, were replaced with acetates. Glu426, which hydrogen-bonds with His484, also forms a salt bridge with Arg52. For this reason, it is considered to be much less basic than Glu150 and Glu370, and thus, it was not included in the models. For the substrate molecule, the whole methyl-substituted π-conjugated system was included in the models, and only the saturated part of the ionone ring was replaced with two methyl groups. The models consist of 126 or 129 atoms, excluding dioxygen, their total charge is 0, and the spin state is quintet (high-spin Fe^{II}). Positions of several atoms, marked with asterisks in Figure 2, were constrained to their coordinates from the crystal structure.

All quantum chemical calculations employing these models were performed with hybrid DFT. The B3LYP exchange-correlation functional in the Jaguar and Gaussian 03 programs was used.[18–21] Geometry optimizations were done with a valence double-zeta basis set coupled with an ef-

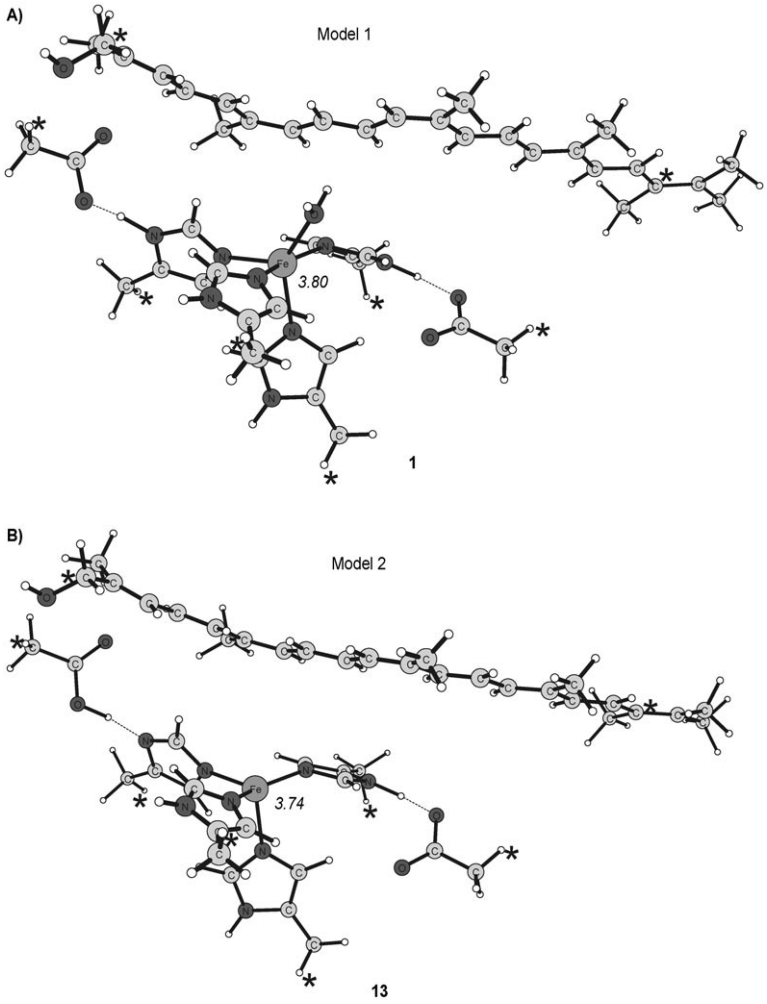

Figure 2. Optimized structures for the two models of the active-site region in the ACO–Fe^{II}-substrate complex. Spin populations are in italics, atoms marked with asterisks were constrained to their positions in the crystal structure.

 © 2008 Wiley-VCH Verlag GmbH & Co. KGaA, Weinheim

fective core potential describing the innermost electrons on iron. This particular basis set is labeled lacvp in Jaguar, and like in our previous studies, the same basis set was used in optimizations performed with Gaussian 03. For the optimized structures, the electronic energy was computed with a bigger basis set of triple-zeta quality with polarization functions on all atoms except iron (lacv3p for iron and cc-pVTZ(−f) for the other atoms).

Due to the size of the system, in most cases only approximate transition structures (TS) were optimized. This was accomplished in the following way: for selected approximate reaction coordinates (interatomic distances) relaxed scans were performed with a step of 0.1 Å for bonds not involving hydrogens and 0.05 Å for X–H distances. Once the maximum energy point (approximate TS) was found, optimizations starting from two points on both sides of the maximum were performed in order to check if the TS found connects the right reactant and product. However, for the rate-limiting step in a given mechanism or model the transition state was fully optimized with Gaussian 03, and the character of the stationary point was checked by a frequency analysis.

To reproduce the polarization effects of the enzyme environment, the self-consistent reaction field implemented in Jaguar was employed.[22,23] The solvent is modeled as a homogenous macroscopic continuum with dielectric constant [ε] = 4.0 and the solute is placed in a cavity contained in this continuous medium. The probe radius used to build the cavity was 1.4 Å. Final energies of the optimized structures were corrected for solvent effects by employing the B3LYP functional and the lacvp basis set.

The zero-energy level corresponds to the separate ACO–Fe^{II}-substrate complex and O_2 in their ground electronic state. Histidine ligands produce a weak ligand field,[24] which results in a high-spin (quintet, S = 2) ground state of the ACO–Fe^{II}-substrate complex, whereas dioxygen has a triplet ground state. Here, a few comments should be made about the calculated energetics of dioxygen binding. First, the energy profiles presented in this contribution do not include entropy effects. Entropy effects are expected to be very similar for all points except the starting point with a free dioxygen. The additional entropy of this point should be around 10 kcal mol^{-1}. When dioxygen becomes bound there is a compensating effect that should be added to the energy curve. In contrast to accurate calculations and experiments, experience has shown that the electronic-structure method employed in this study has a tendency to underestimate the enthalpy of binding of dioxygen and other small molecules.[25] An additional effect comes from protein restrain and van der Waals interactions.[26,27] For simplicity, we have assumed that entropy and these other additional effects essentially cancel each other out, which is why entropy has not been included in the figures. For a more detailed discussion of the accuracy of the computational methodology employed in this work, the Reader is referred to recent reviews.[28,29]

For the two models (**model 1** and **2**) separate zero-energy levels were used, which means that a sum of energies calculated for **1** and O_2 is the zero level for **model 1**, whereas for **model 2** a sum of energies of **13** and O_2 is the reference (zero) point. Thus, it is assumed that the reactants of the two models (species **1** and **13**) have equal stabilities, which is to a good approximation true, because the calculated energy for the reaction: **1**→**13** + H_2O is only +0.7 kcal mol^{-1}.

Results and Discussion

Here, the results obtained with **model 1**, in which the water ligand is coordinated to iron, are presented and discussed first. The data obtained for **model 2** is described in less detail, because the two models gave rather similar results.

Model 1

Binding of dioxygen: The structure of the optimized model for the ACO–Fe^{II}–H_2O-substrate complex **1** is presented in Figure 2A. In this structure the electronic state of the ferrous ion is a high-spin (quintet, S = 2) state, whereas the electronic configuration of the apocarotenoid is a closed-shell singlet, as can be deduced from the calculated atomic spin populations. Because in this model the water ligand is retained when dioxygen binds, two modes of O_2 binding can be envisioned. First, in species **2** the water molecule is shifted to the position *trans* to His304, and dioxygen binds in an end-on fashion at the site *trans* to His183, that is, the site originally occupied by water (Figure 3A). Second, the water molecule remains at its original site and O_2 binds *trans* to His304 (species **II** shown in Figure S3A). In the first binding mode dioxygen is positioned close to the carotenoid substrate, and such an arrangement leads to mechanisms with low activation barriers. On the other hand, binding of O_2 *trans* to His304 is energetically less favorable and it also leads to larger separation between the carotenoid and the dioxygen ligand.

Binding of O_2 *trans* to His183 affords a complex that features a short hydrogen bond between the distal oxygen atom and the water ligand, and an O–O distance typical for a superoxide group (Figure 3A). These geometrical characteristics are paralleled by the atomic spin populations showing that already in the septet spin state (structure not shown), which is directly available for the ground-state reactants, binding of dioxygen promotes one-electron oxidation of carotenoid to a radical cation (car$^{\bullet+}$). The gross spin population for the main-chain carbon atoms of the carotenoid substrate is 0.9, whereas for the O_2 ligand it is 1.1. The calculated energy of this septet complex is +1.8 kcal mol^{-1}. Changing the spin orientation, form alpha to beta, of the unpaired electron on car$^{\bullet+}$ leads to a quintet complex, with energy of +1.4 kcal mol^{-1}, and gross spin populations on car$^{\bullet+}$ and O_2 of −1.0 and +1.0, respectively (Figure 3A). This antiparallel spin arrangement of the unpaired electrons on car$^{\bullet+}$ and O_2 will facilitate formation of a bond between the two radicals. Besides the proper spin polarization, also the geometrical structure of **2** suggests that the progress of the catalytic reaction should be relatively straightforward. It can be noticed in Figure 3A that the distances between the distal (O2) and proximal (O1) atoms of O_2 and C15′ are 2.99 and 3.12 Å, respectively, and O2 is only 1.52 Å away from the hydrogen of the water molecule. Reaction mechanisms taking advantage of these close contacts are described below.

Dioxetane mechanism: The most straightforward mechanism for carotenoid cleavage starts from the quintet complex **2** and involves an attack of the proximal oxygen atom O1 on C15′ (Scheme 3, Figure 4).

The structure of the fully optimized transition state for this process (**TS1**) is shown in Figure 5A and its energy is 15.9 kcal mol^{-1}.

The bond lengths and spin populations reported in this figure indicate that the attack of O1 on C15′ is accompanied by an electron transfer from car$^{\bullet+}$ to the superoxide: relative to **2**, the total spin population decreased from −0.99 to

 © 2008 Wiley-VCH Verlag GmbH & Co. KGaA, Weinheim

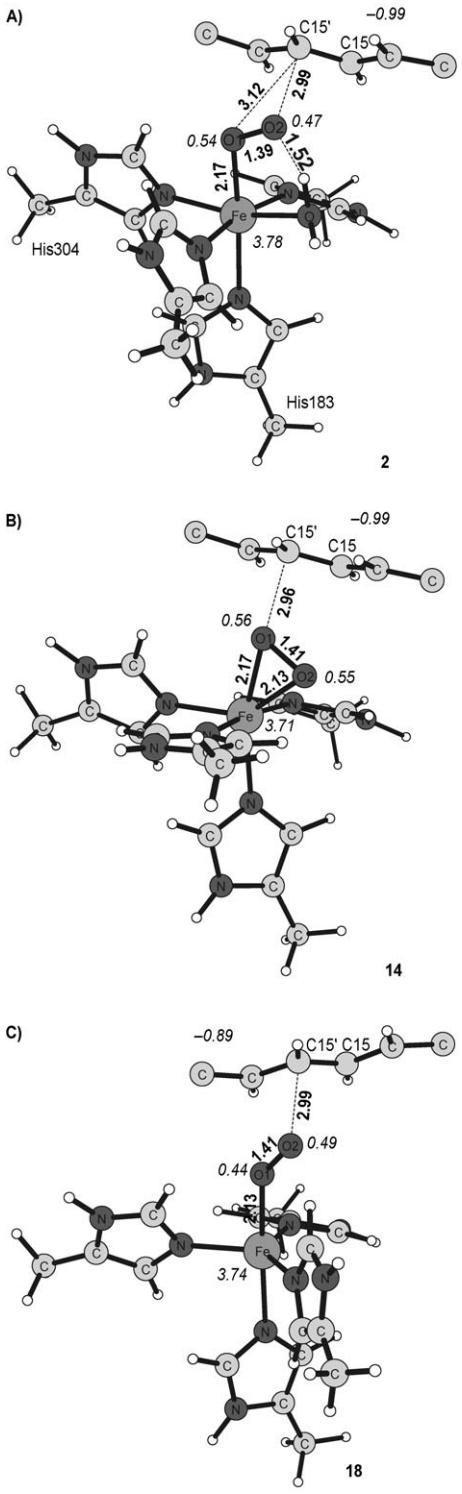

Figure 3. Optimized structures for the dioxygen-bound complexes in the quintet spin state: A) end-on bound complex **2** (**model 1**), B) side-on bound complex **14** (**model 2**), C) end-on bound complex **18** (**model 2**). Distances in Å are in bold, spin populations are in italics. Only the most relevant part of the model is presented.

−0.56 and from 1.1 to 0.48 for car$^{\bullet+}$ and O_2, respectively, whereas the O−O bond lengthened from 1.39 to 1.45 Å.

In the rather unstable product afforded by this attack (**3**, 15.0 kcal mol^{-1}), the bond length and the total spin population for the O_2 group is 1.52 Å and 0.08, whereas the gross spin population on the conjugated π system is only −0.26 (Figure S1 A), which indicates that the transfer of an electron from car$^{\bullet+}$ to O_2 is almost complete.

Importantly for the progress of the reaction, in **3** the distance between the distal oxygen O2 and C15 is only 3.00 Å, and decreasing it to 2.74 Å gives **TS2**, that is, the transition state for the formation of dioxetane (Figure S1 B). The energy of **TS2** is 15.8 kcal mol^{-1}, which is only 0.1 kcal mol^{-1} less than for **TS1**.

Closing the four-membered ring totally quenches the spin populations on O_2 and the carotenoid, and yields the dioxetane intermediate (**4**, −0.3 kcal mol^{-1}). One can notice in Figure 5B that in **4**, one oxygen atom of the dioxetane group (O1) is in contact with the ferrous ion (distance of 2.31 Å), whereas the second oxygen (O2) forms a hydrogen bond with the water ligand. This Fe^{II}−O1 contact is catalytically relevant because in the first step of the decomposition of the dioxetane the O−O bond is cleaved and the presence of the metal ion facilitates this process by lowering the barrier by 13.8 kcal mol^{-1}. More specifically, for the isolated dioxetane intermediate derived from the apocarotenoid substrate, O–O cleavage is homolytic and involves a barrier of 18.4 kcal mol^{-1}. On the other hand, for the ACO active-site model, the O–O cleavage is accompanied by an electron transfer from iron to oxygen O1, which is reduced to the O^- anion coordinating Fe^{III}, and this process reduces the barrier from 18.4 to 4.6 kcal mol^{-1}. The structure of the transition state for the O−O bond cleavage (**TS3**, 4.3 kcal mol^{-1}) is presented in Figure S1 C and demonstrates that a small spin population on O1 and a short Fe–O1 distance are consistent with the Fe→O1 electron transfer during the O−O bond rapture.

Once the O−O bond is cleaved, an intermediate **5** is formed (−20.7 kcal mol^{-1}, Figure 5C) in which the distal oxygen atom (O2) has a clear radical character. From the calculated energy profile (Figure 4) it can be recognized that **5** is a very reactive species. A modest elongation of the C15′−C15 bond, from 1.56 to 1.76 Å, accompanied by an energy increase of only 0.3 kcal mol^{-1}, leads to transition state **TS4** (−20.4 kcal mol^{-1}) for the final cleavage of the organic substrate into the aldehyde products (Figure S1 D). In this step a homolytic cleavage of the C15′−C15 bond is concerted with an electron transfer from the organic intermediate back to iron, which recovers the Fe^{II} catalyst previously oxidized to Fe^{III} during the O−O bond cleavage step. The product complex (**6**, −82.9 kcal mol^{-1}) features two closed-shell aldehyde molecules interacting with the ferrous ion, one directly, and the second one through a hydrogen bond with the water ligand (Figure 5D).

The initial steps of the mechanism described above can be slightly modified by a proton transfer between the water and O_2 ligands (Scheme 3, Figure 4). Starting from the quintet complex **2**, a shift of a proton from the water ligand to the distal oxygen atom O2 involves a small activation barri-

 © 2008 Wiley-VCH Verlag GmbH & Co. KGaA, Weinheim

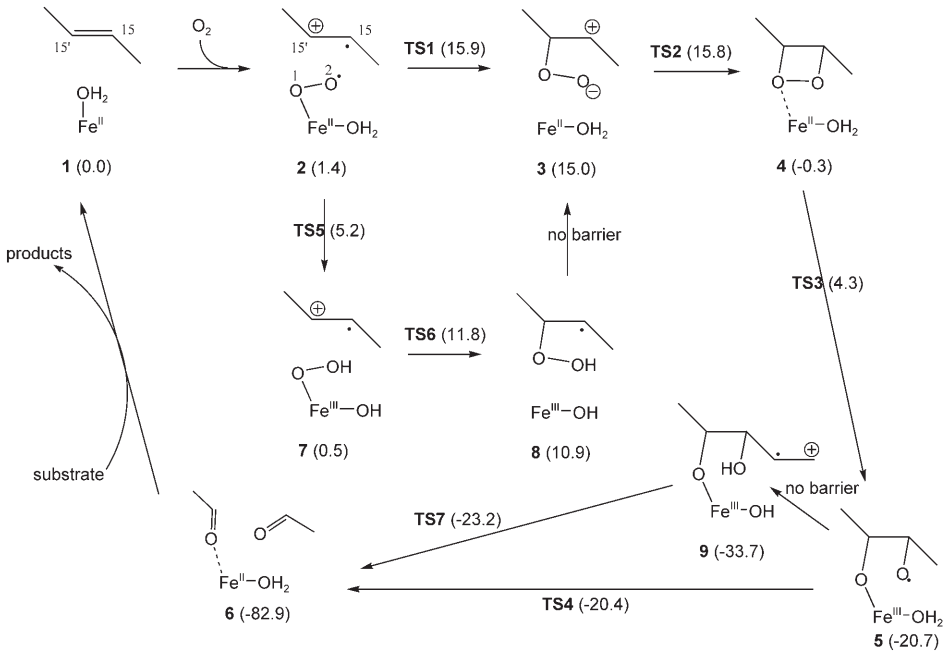

Scheme 3. Dioxetane reaction mechanism investigated for **model 1**.

er (3.8 kcal mol^{-1}) and leads through **TS5** (Figure S1 E) to intermediate **7** (0.5 kcal mol^{-1}, Figure S1 F). A substantial spin population on HOO (0.47) indicates that the hydroperoxo ligand has a noticeable radical character. As for **2**, in **7** the proximal oxygen atom O1 is suitably positioned for an attack at C15′ (O1–C15′ distance of 2.95 Å), but notably, this reaction, leading through **TS6** (Figure S1 G, 11.8 kcal mol^{-1}), involves a markedly lower barrier (Figure 4). Also, the product of the HOO transfer (**8**, 10.9 kcal mol^{-1}) is more stable than the unprotonated (on the O_2 group) counterpart (**3**, 15.0 kcal mol^{-1}). To transform **8** (Figure S1 H) into the dioxetane intermediate, the proton has to be transfered back form the OOH group to the water-derived hydroxide, and the C15–O2 bond has to be formed. The exploration of the potential-energy surface indicates that the proton transfer takes place first. Notably, no TS was found for the proton transfer, because during the scan of the O–H distance the energy increased slowly and monotonically until structure **3** was reached. Thus, it is concluded that **3** is not a stable intermediate, but rather a plateau on the energy surface. Nevertheless, once this structure is formed, the variant of the dioxetane mechanism involving a proton shuttle converges back to the original one. Importantly, from the energy profile shown in Figure 4 it follows that both variants of the dioxetane mechanism feature comparable rate-limiting barriers connected with **TS1** (15.9 kcal mol^{-1}) and **TS2** (15.8 kcal mol^{-1}) for the mechanism not involving and involving proton shuttle, respectively.

In addition to the proton transfers during the initial stages of the dioxetane mechanism, also the final steps can be modified in an analogous way (Scheme 3, Figure 4). Thus, in the O-radical species **5** (Figure 5C), the distal oxygen atom O2 forms a hydrogen bond with the water ligand, and a proton transfer form the water to this oxygen is very easy. A

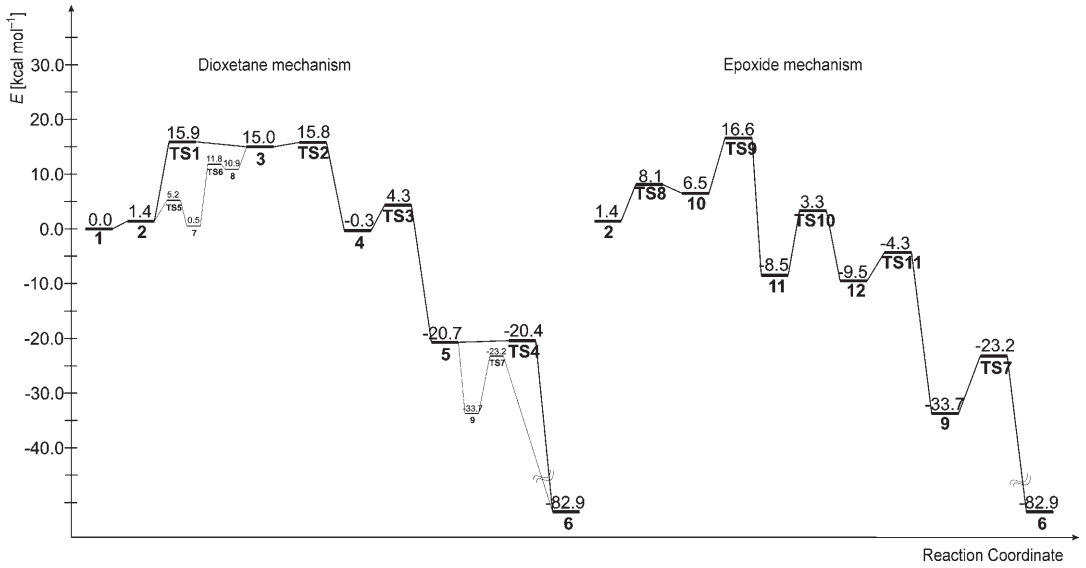

Figure 4. Calculated energy profiles for the mechanisms investigated for **model 1**. Left: dioxetane mechanism, right: epoxide mechanism. For the dioxetane mechanism, steps involving proton exchange between the H_2O and O_2 ligands are shown in small print.

 © 2008 Wiley-VCH Verlag GmbH & Co. KGaA, Weinheim

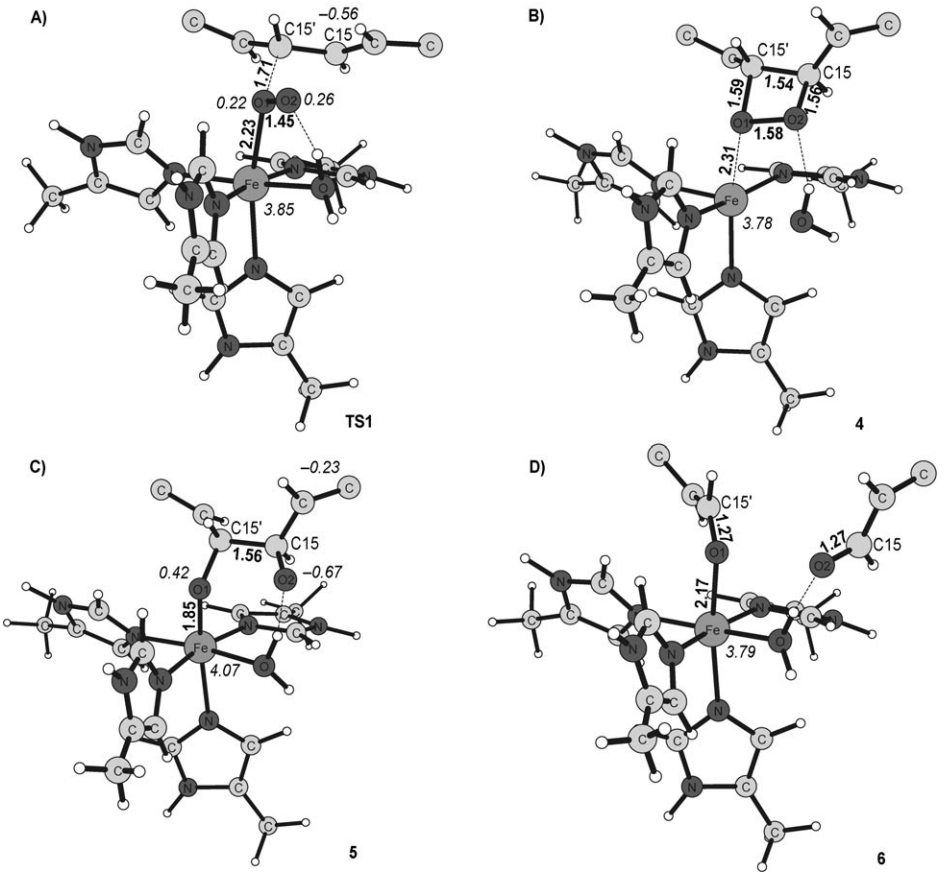

Figure 5. Key structures for the dioxetane reaction mechanism investigated for **model 1**: A) transition state **TS1** for the attack of the proximal oxygen O1 on C15′, B) dioxetane intermediate **4**, C) diolate radical intermediate **5**, D) product complex **6**. Distances in Å are in bold, spin populations are in italics. Only the most relevant part of the model is presented.

TS for this process was located (-22.6 kcal mol^{-1}), but the small activation energy calculated in vacuum (0.9 kcal mol^{-1}) is overcompensated by the negative solvent effect (-2.8 kcal mol^{-1}), and it is concluded that this reaction (**5**→**9**) is spontaneous. The product of the proton transfer (**9**, -33.7 kcal mol^{-1}) is a complex between the high-spin Fe^{III}–OH form of the active site and a monodeprotonated diol whose π system is one-electron oxidized (Figure S1 I). Concerted cleavage of the C15′–C15 bond and a proton transfer back to the water-derived OH ligand leads from **9** through **TS7** (-23.2 kcal mol^{-1}, Figure S1 J) to the final product complex **6**.

Thus, the presence and the acid–base activity of the water ligand slightly modifies the dioxetane mechanism, yet the rate-limiting barrier connected with formation of the dioxetane ring remains unaffected. This is in contrast to the critical role played by the water ligand in the epoxide mechanism discussed below.

Epoxide mechanism: The mechanism involving the epoxide intermediate starts from the quintet species **2** with an attack of the distal oxygen O2 on C15′ (Scheme 4).

In **2** the distance between these two atoms is 2.99 Å and shortening it to 1.80 Å leads to a transition state for the formation of the peroxo bridge between Fe and C15′ (**TS8**, 8.1 kcal mol^{-1}, Figure S2 A).

Already for **TS8** the total spin population on the carotenoid backbone is reduced to -0.8, and it is -0.58 for the product of this attack (**10**, 6.5 kcal mol^{-1}, Figure 6A). These numbers show that the attack of the superoxide group on C15′ is accompanied by a partial oxidation of car$^{\bullet+}$, so that in **10** the C15 branch of the carotenoid has a mixed radical/carbocation character (Scheme 4).

Important geometric features of the peroxo-bridged intermediate **10** are as follows: the proximal oxygen O1 binds to iron with a relatively short bond (1.95 Å), the distal oxygen is only 2.44 Å away from the carbon C15, and the C15-C15′-O2-O1 dihedral angle is $-134°$. These metric characteristics are important because relatively small changes in their values lead to the transition state for the formation of the epoxide intermediate (**TS9**, 16.6 kcal mol^{-1}, Figure 6B). As can be noticed in the figure, in **TS9** the O–O bond is cleaved concertedly with closing the epoxide ring and formation of the oxoferryl group. The value of the C15-C15′-O2-O1 dihedral angle is $-151°$, which means that the bonds cleaved (O–O) and formed (O–C15) are nearly coplanar at the transition state. A similar ar-

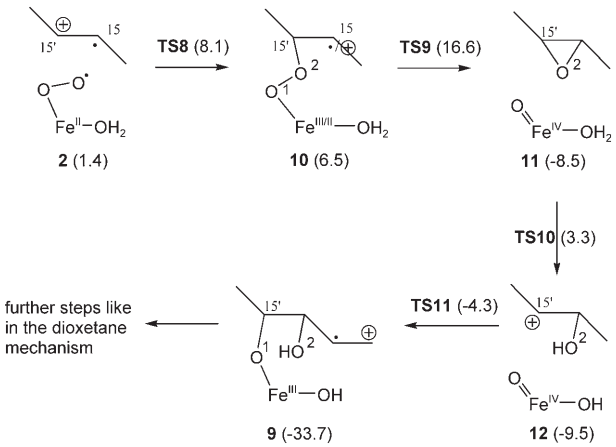

Scheme 4. Epoxide reaction mechanism investigated for **model 1**.

 © 2008 Wiley-VCH Verlag GmbH & Co. KGaA, Weinheim

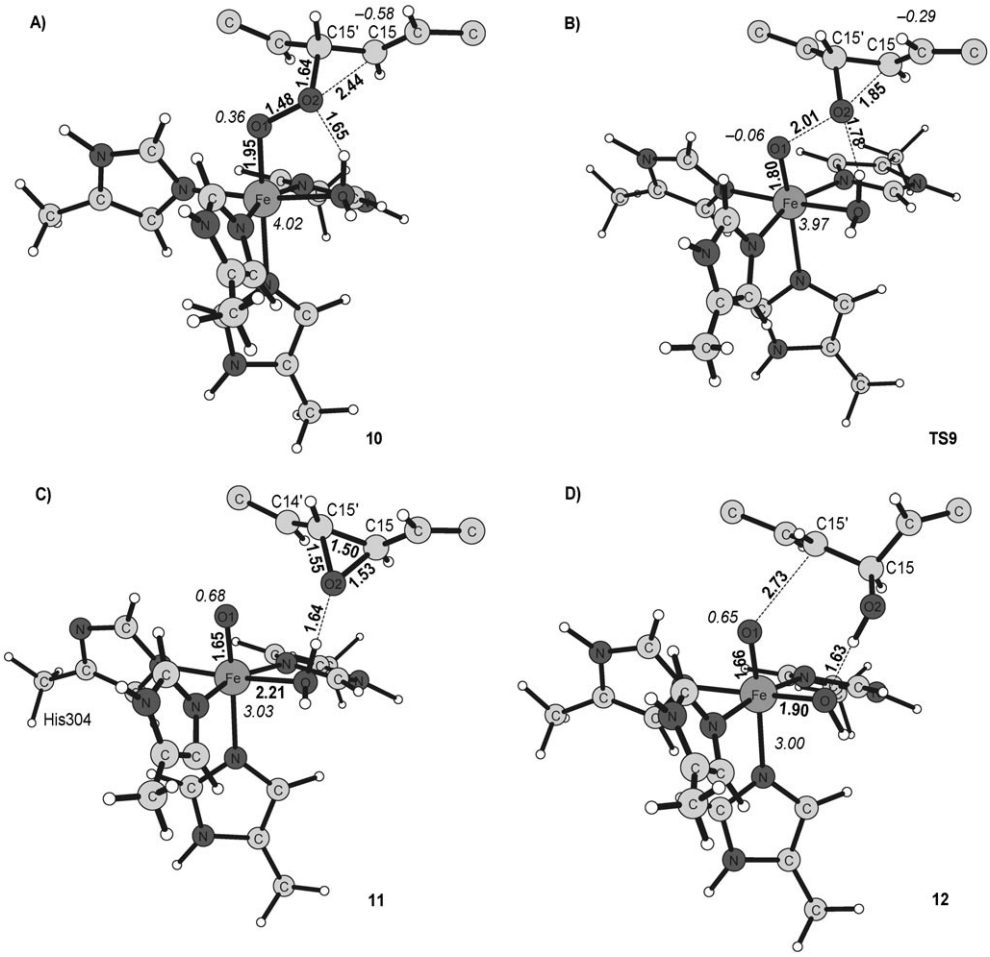

Figure 6. Key structures for the epoxide reaction mechanism investigated for **model 1**: A) peroxo-bridged intermediate **10**, B) transition state for synchronous O–O bond cleavage and the epoxide ring formation **TS9**, C) epoxide intermediate **11**, D) product of the epoxide ring opening **12**. Distances in Å are in bold, spin populations are in italics. Only the most relevant part of the model is presented.

rangement was found previously for the Criegee rearrangement, which is a key step in the reaction mechanism of intradiol dioxygenases.[25]

In the epoxide intermediate (**11**, -8.5 kcal mol^{-1}, Figure 6C) the carotenoid derivative has a closed-shell character (null atomic spin populations), whereas the spin populations on the Fe=O group are typical for the quintet oxoferryl species.[30] Notably, in **11** the epoxide oxygen atom hydrogen-bonds with the water ligand, which suggests that opening of the epoxide ring could be facilitated by a proton transfer from this water. Indeed, the cleavage of the C15′–O bond is coupled to the proton transfer from the water ligand. In the transition state for this reaction (**TS10**, 3.3 kcal mol^{-1}, Figure S2B), the C15′–O2 distance is 1.98 Å, whereas the separation between O2 and the water-ligand hydrogen is only 1.43 Å.

The product of this ring opening (**12**, -9.5 kcal mol^{-1}, Figure 6D) is a hydrogen-bonded complex between a carotenoid-derived carbocation species and a reactive oxoferryl complex, and it is slightly more stable than the epoxide precursor. The distance between the oxo atom O1 and C15′ is only 2.73 Å, and by reducing it to 1.98 Å a transition state for the formation of the C15′–O1 bond is achieved (**TS11**, -4.3 kcal mol^{-1}, Figure S2C). This easy step thus leads to the diolate species **9** (Scheme 4), also encountered in the variant of the dioxetane mechanism involving a proton shuttle, and thus, the following steps of the epoxide mechanism proceed as described in the previous subsection (dioxetane mechanism).

Notably, in the epoxide intermediate **11** the oxo group is rather close to the carotenoid, that is, the O1–C14′ distance is only 2.86 Å, and this opens the possibility for an incorporation of the oxygen across the C14′–C13′ double bond, a reaction that might lead to products not observed for ACO. This alternative reaction channel was investigated for **model 2**, and is discussed below.

Finally, the epoxide ring of **11** could be opened with the participation of an external water molecule, which correspond to the monooxygenase-type reaction previously proposed (Scheme 2). This would most likely follow a general acid-/general base-catalyzed mechanism analogous to that proposed for the limonene-1,2-epoxide hydrolase;[31] that is,

 © 2008 Wiley-VCH Verlag GmbH & Co. KGaA, Weinheim

a water-derived hydroxide attacks carbon C15 (or C15′) from the site opposite to the epoxide oxygen, and the O2 oxyanion produced by opening of the epoxide ring is protonated by the iron-bound water. Such a reaction would lead to a diol intermediate, which could be oxidized subsequently by the oxoferryl species to the aldehyde products (Scheme 2). However, this mechanism requires that the external water is activated by some base, and in the active site of ACO such a group is missing. The site opposite to the epoxide oxygen is lined by hydrophobic residues unable to activate the water molecule. Thus, it is proposed that the monooxygenase mechanism, which involves formation of the diol intermediate through the epoxide hydrolysis, is not realized by ACO, yet some other carotenoid oxygenases might use it, provided they have a necessary basic residue activating a water molecule for a nucleophilic attack on the epoxide.

OH attack: Binding of dioxygen at the site *trans* to His304 leads to species **II** (5.8 kcal mol^{-1}), in which the water ligand is positioned very close (3.10 Å) to carbon C15′ (Figure S3 A). Such an arrangement suggests that a water-derived hydroxide could attack car$^{\bullet+}$ leading to the monooxygenase-type reaction mechanism (Scheme 5).

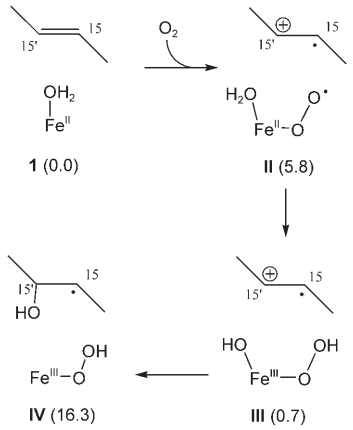

Scheme 5. Initial steps of the alternative mechanism involving attack of the OH anion on the carotenoid radical cation.

The first step of this mechanism would involve a proton transfer from the water to the dioxygen ligand leading to species **III** (0.7 kcal mol^{-1}, Figure S3 B). However, despite the fact that in this intermediate the distance between C15′ and the OH ligand is rather short (3.06 Å), formation of a chemical bond between these two groups is a difficult process. During the scan of the C15′–OH distance the energy rose monotonically, up to 16.3 kcal mol^{-1} for the C–O distance of 1.53 Å (**IV**, Figure S3 C). Thus, **IV** is not a stable intermediate, and a transition state leading from **III** to the next intermediate could be sought starting form the structure of **IV**. The energy of such a TS would most likely be at least a few kcal mol^{-1} higher than the energy of **IV**, which means a barrier of at least 19 kcal mol^{-1} and a process markedly slower than the two mechanisms discussed above. For this reason, the mechanism involving the attack of the water-derived hydroxide on car$^{\bullet+}$ was not studied further and it is considered to be unlikely.

In summary, the computational results obtained for **model 1** indicate that the dioxetane mechanism (Scheme 3) involves the lowest rate-limiting barrier (15.8 kcal mol^{-1}), although the barrier in the epoxide mechanism is only slightly higher (16.6 kcal mol^{-1}). In addition, the epoxide mechanism involves the reactive oxoferryl species, which poses a risk of compromising the product specificity, as discussed below.

Model 2

Binding of dioxygen: If the dioxygen binding is accompanied by the release of the water molecule from the first coordination shell of the iron (**model 2**), the O_2 molecule can bind to Fe in either an end-on or a side-on fashion. For the reactive quintet state, the two binding modes lead to complexes with energies of 9.4 and 4.0 kcal mol^{-1}, for the end-on and side-on complex, respectively. In the end-on complex **18** (Figure 3C), the distal oxygen atom O2 is 2.99 Å away from C15′, whereas for the side-on complex the corresponding O1–C15′ distance is 2.96 Å (Figure 3B). Like in **model 1**, two different mechanisms are initiated by the attack of these oxygen atoms on C15′ and they are presented in the two subsequent subsections.

Dioxetane mechanism: The absence of the water ligand in **model 2** modifies only slightly the dioxetane mechanism presented above for **model 1**. The most notable difference is the absence of a stable peroxide intermediate, analogous to **3**, that is, as shown in Scheme 6 and Figure 7, the dioxetane intermediate **15** is formed directly from the side-on complex **14**.

This reaction goes through **TS12** (16.4 kcal mol^{-1}, Figure 8A) connecting the side-on intermediate **14** with the dioxetane species **15** (4.4 kcal mol^{-1}, Figure 8B).

Concerning the structure and the electronic state, **TS12** resembles **TS2**, that is, in both cases the O1−C15′ bond is al-

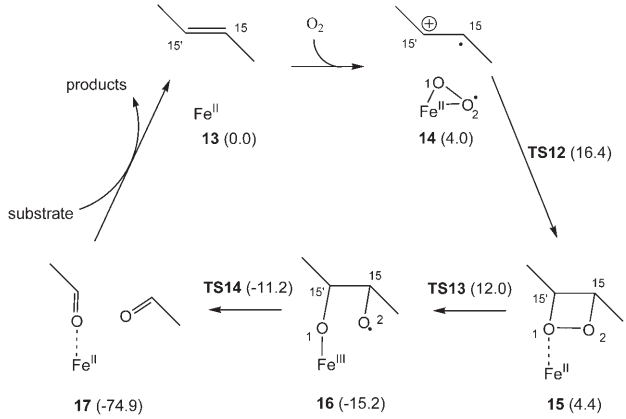

Scheme 6. Dioxetane reaction mechanism investigated for **model 2**.

© 2008 Wiley-VCH Verlag GmbH & Co. KGaA, Weinheim

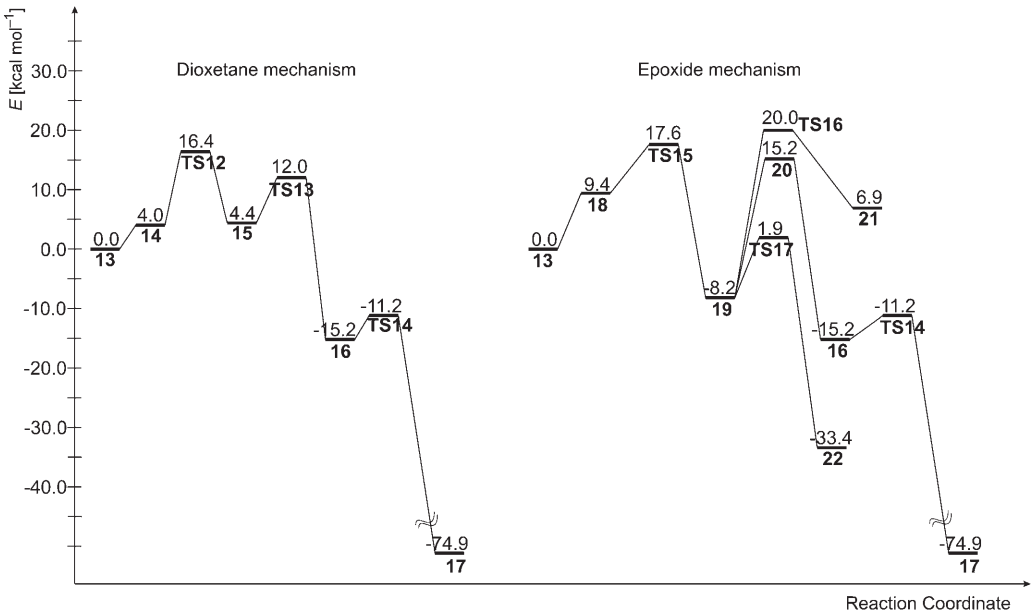

Figure 7. Calculated energy profiles for the mechanisms investigated for **model 2**. Left: dioxetane mechanism, right: epoxide mechanism.

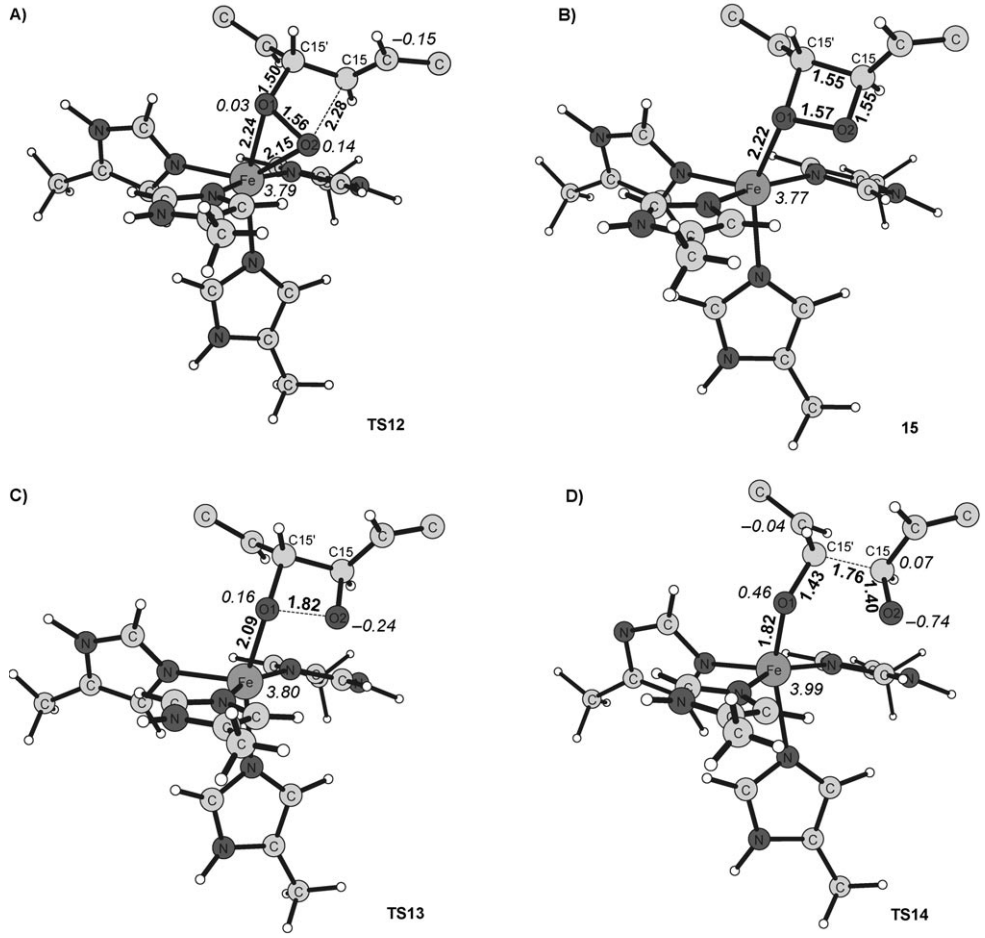

Figure 8. Key structures for the dioxetane reaction mechanism investigated for **model 2**: A) transition state **TS12** for the attack of the oxygen on car$^{\bullet+}$, B) dioxetane intermediate **15**, C) transition state for the O–O bond cleavage **TS13**, D) transition state for the C–C bond cleavage **TS14**. Distances in Å are in bold, spin populations are in italics. Only the most relevant part of the model is presented.

 © 2008 Wiley-VCH Verlag GmbH & Co. KGaA, Weinheim

ready developed and the organic substrate has a carbocationic character, as can be inferred from the small total spin population. The chemistry that occurs at those points on the potential-energy surfaces is a nucleophilic attack of the peroxide anion (O2) on the carbocation (C15).

In the dioxetane intermediate (**15**, 4.4 kcal mol^{-1}, Figure 8B) one oxygen atom from the four-membered ring (O1) makes a close contact with the ferrous ion (2.22 Å), which, as discussed at length for **model 1**, facilitates the O–O bond cleavage. This easy reaction, proceeding through **TS13** (12.0 kcal mol^{-1}, Figure 8C), leads to a diolate radical species **16** (−15.2 kcal mol^{-1}, Figure S4 A), which in turn, decays through the C15′–C15 bond cleavage (**TS14**, −11.2 kcal mol^{-1}, Figure 8D) to the final dialdehyde product complex **17** (−74.9 kcal mol^{-1}, Figure S4 B).

Epoxide mechanism: In similarity to the dioxetane mechanism (**model 2**), the absence of the water ligand destabilizes the peroxo-bridged intermediate, analogous to **10**, and in the epoxide mechanism for **model 2** the end-on complex **18** is connected directly with the epoxide intermediate **19** via **TS15** (Scheme 7, Figures 7 and 9A).

This step involves an activation barrier of 17.6 kcal mol^{-1}, which is only 1 kcal mol^{-1} higher than for **model 1**. However, this is not the only difference compared to the epoxide

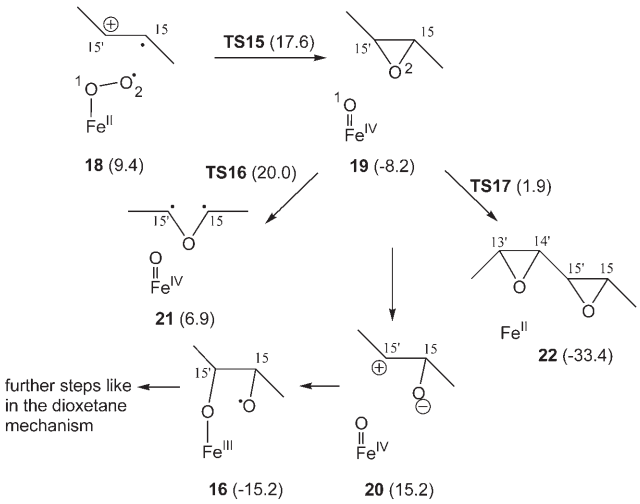

Scheme 7. Epoxide reaction mechanism investigated for **model 2**.

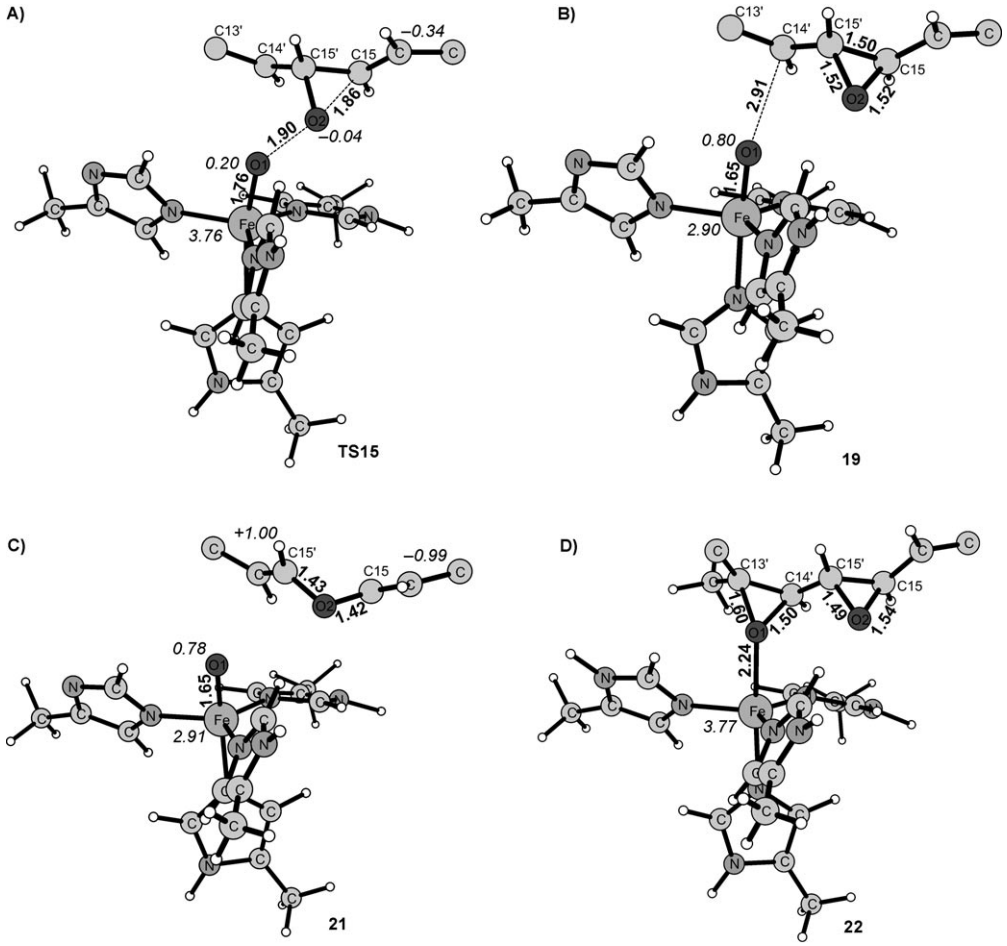

Figure 9. Key structures for the epoxide reaction mechanism investigated for **model 2**: A) transition state **TS15** for the synchronous O–O cleavage and the epoxide ring formation, B) epoxide intermediate **19**, C) biradical species **21**, D) double epoxide product **22**. Distances in Å are in bold, spin populations are in italics. Only the most relevant part of the model is presented.

 © 2008 Wiley-VCH Verlag GmbH & Co. KGaA, Weinheim

mechanism for **model 1**. Most importantly, in **model 1** the cleavage of the C15′−O2 bond in the epoxide ring is facilitated by a proton transfer from the water ligand (Scheme 4, reaction: **11**→**TS10**→**12**) and involves a modest barrier of 11.8 kcal mol^{-1}. The lack of the water ligand in **model 2** practically disables this reaction, because the unsupported opening of the epoxide ring (Scheme 7, **19**→**20**) is endothermic by 23.4 kcal mol^{-1}. Similarly, the homolytic cleavage of the C15′−C15 bond in the epoxide intermediate, **19**→**21**, involves a prohibitively high activation barrier of 28.2 kcal mol^{-1}. On the other hand, in **19** (Figure 9B), the reactive oxo atom lies very close to the C13′−C14′ double bond, suggesting that another reaction channel might be possible. Indeed, insertion of the oxo atom (O1) across the C13′−C14′ bond involves a modest barrier of 10.1 kcal mol^{-1} connected with **TS17** (Figure S5C) and it is irreversible, because the double epoxide product **22** (Figure 9D) is more stable by 25.2 kcal mol^{-1} than the epoxide intermediate **19** (Figure 7).

In summary, the results obtained for **model 2** suggest that if the water ligand is absent in the iron coordination shell, the most favorable reaction path for carotenoid cleavage follows the dioxetane mechanism, which involves the lowest activation barrier and guarantees the necessary product specificity.

Conclusions

The reaction mechanism for the oxidative cleavage of apocarotenoids was investigated by applying the DFT (B3LYP) computational method to two realistic models of the ACO active site, that differ by the presence (**model 1**) or absence (**model 2**) of the water ligand in the coordination shell of iron. The results presented in this work suggest that the dioxetane mechanism (Scheme 3 or Scheme 6), which corresponds to the dioxygenase mechanism proposed by Schmidt et al. (Scheme 2),[16] is the slightly preferred mechanism for the studied apocarotenoid oxygenase. This mechanism involves the lowest activation barrier and in a straightforward way guarantees the proper product specificity. However, the epoxide mechanism involves a barrier only slightly higher, and when the water ligand binds to iron (**model 1**, Scheme 4), it may also lead to the proper products of the cleavage. In the specific case of ACO, the presence of the Thr136 side chain close to the site *trans* to His304 (Figure 1) most likely disfavors binding of a water molecule at this site, and thus, the water is released upon O_2 binding and the reaction follows the dioxetane mechanism for **model 2** (Scheme 6).

Acknowledgement

T.B. acknowledges the support from the Polish State Committee for Scientific Research (Grant N204 173 31/3823).

[1] M. E. Auldridge, D. R. McCarty, H. J. Klee, *Curr. Opin. Plant. Biol.* **2006**, *9*, 315–321.
[2] W. Stahl, H. Sies, *Biochim. Biophys. Acta* **2005**, *1740*, 101–107.
[3] J. von Lintig, S. Hessel, A. Isken, C. Kiefer, J. M. Lampert, O. Voolstra, K. Vogt, *Biochim. Biophys. Acta* **2005**, *1740*, 122–131.
[4] J. Olson, O. Hayaishi, *Proc. Natl. Acad. Sci. USA* **1965**, *54*, 1364–1370.
[5] S. Schwartz, B. Tan, D. Gage, J. Zeevaart, D. McCarty, *Science* **1997**, *276*, 1872–1874.
[6] J. von Lintig, K. Vogt, *J. Biol. Chem.* **2000**, *275*, 11915–11920.
[7] T. Redmond, S. Gentleman, T. Duncan, S. Yu, B. Wiggert, E. Gantt, F. Cunningham, *J. Biol. Chem.* **2001**, *276*, 6560–6565.
[8] A. Wyss, G. Wirtz, W.-D. Woggon, R. Brugger, M. Wyss, A. Friedlein, H. Bachmann, W. Hunziker, *Biochem. Biophys. Res. Commun.* **2000**, *271*, 334–336.
[9] A. Wyss, G. Wirtz, W.-D. Woggon, R. Brugger, M. Wyss, A. Friedlein, G. Riss, H. Bachmann, W. Hunziker, *Biochem. J.* **2001**, *354*, 521–529.
[10] C. Kiefer, S. Hessel, J. Lampert, K. Vogt, M. Lederer, D. Breithaupt, J. von Lintig, *J. Biol. Chem.* **2001**, *276*, 14110–14116.
[11] S. Ruch, P. Beyer, H. Ernst, S. Al-Babili, *Mol. Microbiol.* **2005**, *55*, 1015–1024.
[12] D. Kloer, G. Schulz, *Cell Mol. Life Sci.* **2006**, *63*, 2291–2303.
[13] G. Giuliano, S. Al-Babili, J. von Lintig, *Trends Plant. Sci.* **2003**, *8*, 145–149.
[14] G. Giuliano, C. Rosati, P. M. Bramley, *Trends Biotechnol.* **2003**, *21*, 513–516.
[15] M. G. Leuenberger, C. Engeloch-Jarret, W.-D. Woggon, *Angew. Chem.* **2001**, *113*, 2683–2687; *Angew. Chem. Int. Ed.* **2001**, *40*, 2613–2617.
[16] H. Schmidt, R. Kurtzer, W. Eisenreich, W. Schwab, *J. Biol. Chem.* **2006**, *281*, 9845–9851.
[17] D. P. Kloer, S. Ruch, S. Al-Babili, P. Beyer, G. E. Schulz, *Science* **2005**, *308*, 267–269.
[18] A. D. J. Becke, *J. Chem. Phys.* **1993**, *98*, 5648–5652.
[19] C. Lee, W. Yang, R. G. Parr, *Phys. Rev. B* **1988**, *37*, 785–789.
[20] Schrödinger, Inc., *JAGUAR 5.5* (Portland, Oregon), **2005**.
[21] *Gaussian 03*, *Revision B.03*, M. J. Frisch, G. W. Trucks, H. B. Schlegel, G. E. Scuseria, M. A. Robb, J. R. Cheeseman, J. A. Montgomery, Jr., T. Vreven, K. N. Kudin, J. C. Burant, J. M. Millam, S. S. Iyengar, J. Tomasi, V. Barone, B. Mennucci, M. Cossi, G. Scalmani, N. Rega, G. A. Petersson, H. Nakatsuji, M. Hada, M. Ehara, K. Toyota, R. Fukuda, J. Hasegawa, M. Ishida, T. Nakajima, Y. Honda, O. Kitao, H. Nakai, M. Klene, X. Li, J. E. Knox, H. P. Hratchian, J. B. Cross, V. Bakken, C. Adamo, J. Jaramillo, R. Gomperts, R. E. Stratmann, O. Yazyev, A. J. Austin, R. Cammi, C. Pomelli, J. W. Ochterski, P. Y. Ayala, K. Morokuma, G. A. Voth, P. Salvador, J. J. Dannenberg, V. G. Zakrzewski, S. Dapprich, A. D. Daniels, M. C. Strain, O. Farkas, D. K. Malick, A. D. Rabuck, K. Raghavachari, J. B. Foresman, J. V. Ortiz, Q. Cui, A. G. Baboul, S. Clifford, J. Cioslowski, B. B. Stefanov, G. Liu, A. Liashenko, P. Piskorz, I. Komaromi, R. L. Martin, D. J. Fox, T. Keith, M. A. Al-Laham, C. Y. Peng, A. Nanayakkara, M. Challacombe, P. M. W. Gill, B. Johnson, W. Chen, M. W. Wong, C. Gonzalez, J. A. Pople, Gaussian, Inc., Wallingford CT, **2003**.
[22] D. J. Tannor, B. Marten, R. Murphy, R. A. Friesner, D. Sitkoff, A. Nicholls, M. Ringnalda, W. A. Goddard III, B. Honig, *J. Am. Chem. Soc.* **1994**, *116*, 11875–11882.
[23] B. Marten, K. Kim, C. Cortis, R. A. Friesner, R. Murphy, M. Ringnalda, D. Sitkoff, B. Honig, *J. Phys. Chem.* **1996**, *100*, 11775–11788.
[24] E. S. Solomon, T. C. Brunold, M. I. Davis, J. N. Kemsley, S. K. Lee, N. Lehnert, F. Neese, A. J. Skulan, Y. S. Yang, J. Zhou, *Chem. Rev.* **2000**, *100*, 235–349.
[25] T. Borowski, P. E. M. Siegbahn, *J. Am. Chem. Soc.* **2006**, *128*, 12941–12953.
[26] M. Lundberg, K. Morokuma, *J. Phys. Chem. B* **2007**, *111*, 9380–9389.

 © 2008 Wiley-VCH Verlag GmbH & Co. KGaA, Weinheim

[27] M. Wirstam, S. J. Lippard, R. A. Friesner, *J. Am. Chem. Soc.* **2003**, *125*, 3980–3987.
[28] P. E. M. Siegbahn, *J. Biol. Inorg. Chem.* **2006**, *11*, 695–701.
[29] P. E. M. Siegbahn, T. Borowski, *Acc. Chem. Res.* **2006**, *39*, 729–738.
[30] A. Bassan, M. R. Blomberg, T. Borowski, P. E. M. Siegbahn, *J. Inorg. Biochem.* **2006**, *100*, 727–743.
[31] K. H. Hopmann, B. M. Hallberg, F. Himo, *J. Am. Chem. Soc.* **2005**, *127*, 14339–14347.

Received: August 28, 2007
Revised: November 10, 2007
Published online: January 7, 2008

 © 2008 Wiley-VCH Verlag GmbH & Co. KGaA, Weinheim